

# A Broadband Approach to Axion Dark Matter Detection

Yonatan Kahn,<sup>1,\*</sup> Benjamin R. Safdi,<sup>2,†</sup> and Jesse Thaler<sup>2,‡</sup>

<sup>1</sup>*Department of Physics, Princeton University, Princeton, NJ 08544, U.S.A.*

<sup>2</sup>*Center for Theoretical Physics, Massachusetts Institute of Technology, Cambridge, MA 02139, U.S.A.*

(Dated: April 15, 2022)

When ultralight axion dark matter encounters a static magnetic field, it sources an effective electric current that follows the magnetic field lines and oscillates at the axion Compton frequency. We propose a new experiment to detect this axion effective current. In the presence of axion dark matter, a large toroidal magnet will act like an oscillating current ring, whose induced magnetic flux can be measured by an external pickup loop inductively coupled to a SQUID magnetometer. We consider both resonant and broadband readout circuits and show that a broadband approach has advantages at small axion masses. We estimate the reach of this design, taking into account the irreducible sources of noise, and demonstrate potential sensitivity to axion dark matter with masses in the range of  $10^{-13}$  eV to  $10^{-6}$  eV, particularly the QCD axion with a GUT-scale decay constant.

A broad class of well-motivated dark matter (DM) models consist of light pseudoscalar particles  $a$  coupled weakly to electromagnetism [1–3]. The most famous example is the QCD axion [4–7], which was originally proposed to solve the strong CP problem. More generally, string compactifications often predict a large number of axion-like particles (ALPs) [8], with Planck-suppressed couplings to electric ( $\mathbf{E}$ ) and magnetic ( $\mathbf{B}$ ) fields of the form  $a \mathbf{E} \cdot \mathbf{B}$ . Unlike QCD axions, generic ALPs do not necessarily couple to the QCD operator  $G\tilde{G}$ , where  $G$  is the QCD field strength. The masses and couplings of ALP DM candidates are relatively unconstrained by theory or experiment (see [9–11] for reviews). It is therefore important to develop search strategies that cover many orders of magnitude in the axion parameter space.

The ADMX experiment [12–14] has already placed stringent constraints on axion DM in a narrow mass range around  $m_a \sim \text{few} \times 10^{-6}$  eV. However, ADMX is only sensitive to axion DM whose Compton wavelength is comparable to the size of the resonant cavity. For the QCD axion, the axion mass  $m_a$  is related to the Peccei-Quinn (PQ) symmetry-breaking scale  $f_a$  via

$$f_a m_a \simeq f_\pi m_\pi, \quad (1)$$

where  $m_\pi \approx 140$  MeV ( $f_\pi \approx 92$  MeV) is the pion mass (decay constant). Lighter QCD axion masses therefore correspond to higher-scale axion decay constants  $f_a$ . The GUT scale ( $f_a \sim 10^{16}$  GeV,  $m_a \sim 10^{-9}$  eV) is particularly well motivated, but well beyond the reach of ADMX as such small  $m_a$  would require much larger cavities. More general ALPs can also have lighter masses and larger couplings than in the QCD case.

In this letter, we propose a new experimental design for axion DM detection that targets the mass range  $m_a \in [10^{-13}, 10^{-6}]$  eV. Like ADMX, this design exploits the fact that axion DM, in the presence of a static magnetic field, produces response electromagnetic fields that oscillate at the axion Compton frequency. Whereas ADMX is based on resonant detection of a cavity excitation, our design is based on broadband (or resonant)

detection of an oscillating magnetic flux with sensitive magnetometers, sourced by an axion effective current. Our static magnetic field is generated by a superconducting toroid, which has the advantage that the flux readout system can be external to the toroid, in a region of ideally zero static field. Crucially, this setup can probe axions whose Compton wavelength is much larger than the size of the toroid. If this experiment were built, we propose the acronym ABRACADABRA, for “A Broadband/Resonant Approach to Cosmic Axion Detection with an Amplifying B-field Ring Apparatus.”

For ultralight (sub-eV) axion DM, it is appropriate to treat  $a$  as a coherent classical field, since large DM number densities imply macroscopic occupation numbers for each quantum state. Solving the classical equation of motion with zero DM velocity yields

$$a(t) = a_0 \sin(m_a t) = \frac{\sqrt{2\rho_{\text{DM}}}}{m_a} \sin(m_a t), \quad (2)$$

where  $\rho_{\text{DM}} \approx 0.3$  GeV/cm<sup>3</sup> is the local DM density [15].<sup>1</sup> Through the coupling to the QED field strength  $F_{\mu\nu}$ ,

$$\mathcal{L} \supset -\frac{1}{4} g_{a\gamma\gamma} a F_{\mu\nu} \tilde{F}^{\mu\nu}, \quad (3)$$

a generic axion will modify Maxwell’s equations, and Ampère’s circuit law becomes [16]

$$\nabla \times \mathbf{B} = \frac{\partial \mathbf{E}}{\partial t} - g_{a\gamma\gamma} \left( \mathbf{E} \times \nabla a - \mathbf{B} \frac{\partial a}{\partial t} \right). \quad (4)$$

For the QCD axion,  $g_{a\gamma\gamma} = g \alpha_{\text{EM}} / (2\pi f_a)$ , where  $\alpha_{\text{EM}}$  is the electromagnetic fine-structure constant and  $g$  is an order-1 number equal to  $\sim 0.75$  ( $-1.92$ ) for the DFSZ model [17, 18] (KSVZ model [19, 20]). Thus, in the presence of a static magnetic background  $\mathbf{B}_0$ , there is an axion-sourced effective current

<sup>1</sup> The local virial DM velocity  $v \sim 10^{-3}$  will give small spatial gradients  $\nabla a \propto v$ .

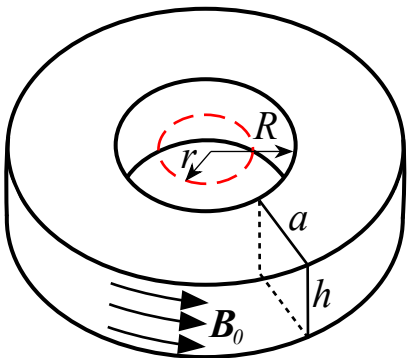


Figure 1. A toroidal geometry to generate a static magnetic field  $\mathbf{B}_0$ . The dashed red circle shows the location of the superconducting pickup loop of radius  $r \leq R$ .

$$\mathbf{J}_{\text{eff}} = g_{a\gamma\gamma} \sqrt{2\rho_{\text{DM}}} \cos(m_a t) \mathbf{B}_0. \quad (5)$$

This effective current then sources a real magnetic field, oscillating at frequency  $m_a$ , that is perpendicular to  $\mathbf{B}_0$ .

Our proposed design is shown schematically in Fig. 1.<sup>2</sup> The static magnetic field  $\mathbf{B}_0$  is generated by a constant current in a superconducting wire wrapping a toroid, and the axion effective current is detected with a superconducting pickup loop in the toroid hole. In the absence of axion DM (or noise), there is no magnetic flux through the pickup loop. With axion DM, there will be an oscillating magnetic flux through the pickup loop proportional to  $\sqrt{\rho_{\text{DM}}}$ . We consider two distinct circuits for reading out the signal, both based on a superconducting quantum interference device (SQUID). The broadband circuit uses a untuned magnetometer in an ideally zero-resistance setup, while the resonant circuit uses a tuned magnetometer with irreducible resistance. Both readout circuits can probe multiple orders of magnitude in the axion DM parameter space, though the broadband approach has increased sensitivity at low axion masses.

A related proposal, utilizing the axion effective current, was put forth recently by [22] (see also [23] for a preliminary proposal and [24] for a similar design for detecting dark photon DM). That design was based on a solenoidal magnetic field, with the pickup loop located inside of the solenoid, and focused on resonant readout using an LC circuit. The design presented here offers a few advantages. First, the toroidal geometry significantly reduces fringe fields compared to a solenoidal geometry. Second, the pickup loop is located in an ideally zero-field region, outside of the toroidal magnetic field  $\mathbf{B}_0$ , which should help reduce flux noise. Third, as we will show, broadband readout has significant advantages over resonant readout

<sup>2</sup> This design is inspired by cryogenic current comparators [21], which are used for measuring real currents. The key difference here is the static external field  $\mathbf{B}_0$ .

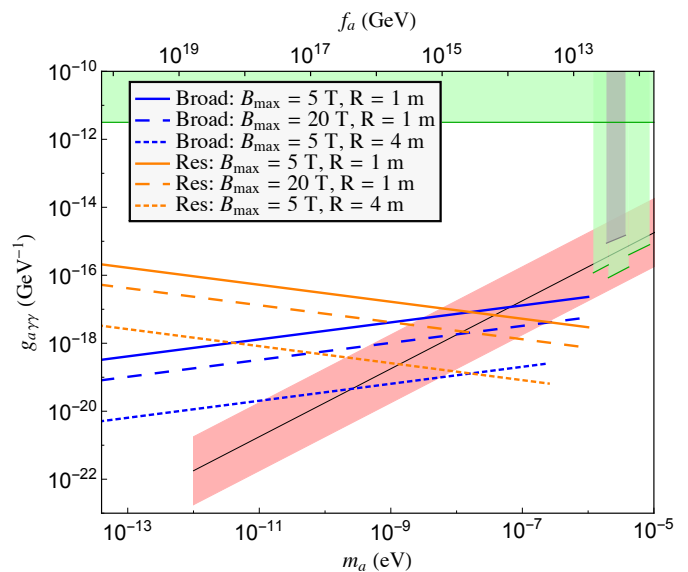


Figure 2. Anticipated reach in the  $g_{a\gamma\gamma}$  vs.  $m_a$  plane for the broadband (Broad) and resonant (Res) strategies. The benchmark parameters are  $T = 0.1$  K and  $r = h = a = R$  (see Fig. 1). The total measurement time for both strategies is  $t = 1$  year, where the resonant experiment scans from 10 Hz to 100 MHz. The expected parameters for the QCD axion are shown in shaded red, with the corresponding decay constant  $f_a$  on the top horizontal axis. The projected sensitivities of IAXO [36] and ADMX [14] are shown shaded in light green. Published limits from ADMX [13] are shown in grey.

at low axion masses. Our proposal is complementary to the recently-proposed CASPER experiment [25], which probes a similar range of axion masses but measures the coupling to nuclear electric dipole moments rather than the coupling to QED. See [26–35] for other proposals to detect axion DM.

For concreteness, our sensitivity studies are based on a toroid of rectangular cross section (height  $h$ , width  $a$ ) and inner radius  $R$ , as illustrated in Fig. 1. The magnetic field inside the toroid volume is

$$\mathbf{B}_0(s) = B_{\text{max}} \frac{R}{s} \hat{\phi}, \quad (6)$$

where  $s$  is the distance from the central axis of the toroid,  $\hat{\phi}$  is the azimuthal direction, and  $B_{\text{max}}$  is the magnitude of  $\mathbf{B}_0$  at the inner radius. The flux through the pickup loop of radius  $r \leq R$  can be written as

$$\Phi_{\text{pickup}}(t) = g_{a\gamma\gamma} B_{\text{max}} \sqrt{2\rho_{\text{DM}}} \cos(m_a t) V_B. \quad (7)$$

The effective volume containing the external  $\mathbf{B}$ -field is

$$V_B = \int_0^r dr' \int_R^{R+a} ds \int_0^{2\pi} d\theta \frac{Rhr'(s - r' \cos \theta)}{\tilde{r}^2 \sqrt{h^2 + 4\tilde{r}^2}}, \quad (8)$$

with  $\tilde{r}^2 \equiv s^2 + r'^2 - 2sr' \cos \theta$ , and we have assumed  $2\pi/m_a \gtrsim r, R, h, a$  such that the quasi-static approximation holds. We focus on a meter-sized experiment for

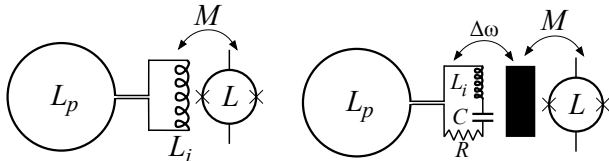


Figure 3. Schematics of our readout circuits. **Left:** broadband (untuned magnetometer). The pickup loop  $L_p$  is placed in the toroid hole as in Fig. 1 and connected in series with an input coil  $L_i$ , which has mutual inductance  $M$  with the SQUID of self-inductance  $L$ . **Right:** resonant (tuned magnetometer).  $L_p$  is now in series with both  $L_i$  and a tunable capacitor  $C$ . A “black box” feedback circuit modulates the bandwidth  $\Delta\omega$  and has mutual inductance  $M$  with the SQUID.

$m_a \lesssim 10^{-6}$  eV and verified numerically that retarded-time effects are negligible for our benchmarks.<sup>3</sup> Throughout, we consider a fiducial geometry with  $r = h = a = R$ , in which case  $V_B/R^3 \approx 0.88$ . As an example of the magnitude of the generated fields, the average  $B$ -field sourced by a GUT-scale KSVZ axion ( $f_a = 10^{16}$  GeV) with  $r = 4$  m and  $B_{\max} = 5$  T is  $1.4 \times 10^{-23}$  T. To detect such a small  $B$ -field at this frequency, we need a flux noise sensitivity of  $8.4 \times 10^{-20}$  Wb/ $\sqrt{\text{Hz}}$  for a measurement time of 1 year in a broadband strategy (see below). The anticipated reach for various  $R$  and  $B_{\max}$  is summarized in Fig. 2.

*Broadband approach*—In an untuned magnetometer, a change in flux through the superconducting pickup loop induces a supercurrent in the loop. As shown in Fig. 3 (left), the pickup loop (inductance  $L_p$ ) is connected in series with an input coil  $L_i$ , which is inductively coupled to the SQUID (inductance  $L$ ) with mutual inductance  $M$ . The flux through the SQUID is maximized when  $L_i \approx L_p$ , which can be achieved by adjusting the number of turns  $N_i$  in the input coil. Writing  $L_i = \alpha^2 N_i^2 L$  and  $M = \alpha^2 N_i L$ , the flux through the SQUID is proportional to the flux through the pickup loop [37]:

$$\Phi_{\text{SQUID}} \approx \frac{\alpha}{2} \sqrt{\frac{L}{L_p}} \Phi_{\text{pickup}}. \quad (9)$$

Here  $\alpha$  is an order-1 number, with  $\alpha^2 \approx 0.5$  in typical SQUID geometries [38].

Clearly, the flux through the SQUID will be maximized for  $L$  as large as possible and  $L_p$  as small as possible. A typical SQUID has inductance  $L = 1$  nH. A superconducting pickup loop of wire radius  $\phi = 1$  mm and loop radius  $r = 1$  m has geometric inductance of [39]

$$L_p = r(\ln(8r/\phi) - 2) \approx 9 \mu\text{H}, \quad (10)$$

<sup>3</sup> However, retarded-time effects are likely important for axion wavelengths much smaller than the size of the experiment.

but this can be reduced by connecting  $N_p$  smaller pickup loops in parallel.<sup>4</sup> With  $N_p = 100$  loops, each of radius 10 cm, and  $\alpha^2 = 0.5$ , one can achieve  $\Phi_{\text{SQUID}} \approx 0.1 \Phi_{\text{pickup}}$ , which we take as our benchmark.<sup>5</sup> Since the pickup loop area is much larger than the magnetometer area, the  $B$ -field felt by the SQUID is significantly enhanced compared to the axion-induced field in the pickup loop. To achieve inductance matching, we take  $N_i = 5$  turns in the input coil. Both the  $B$ -field enhancement and the strategy for reducing  $L_p$  take advantage of the large spatial coherence length of the axion signal, which is  $\lambda \sim 2\pi/(m_a v) \gg 1$  m in the mass range of interest [28].

To assess the sensitivity of the untuned magnetometer to the axion-sourced oscillating flux in (7), we must characterize the noise of the circuit. In a pure superconducting circuit, there is zero noise in the pickup loop and input coil, and the only source of noise is in the SQUID, with contributions from thermal fluctuations of both voltage and current. Despite their thermal origin, we will refer to these as “magnetometer noise” to distinguish them from noise in the pickup loop circuit (which dominates in the resonant case below). At cryogenic temperatures ( $T \lesssim 60$  mK), thermal current and voltage noise are subdominant to the current shot noise  $S_{J,0}$  in the SQUID tunnel junctions [38], which sets an absolute (temperature-independent) floor for the magnetometer noise. See the appendix for a more detailed discussion of noise in a real implementation of this design.

A typical, temperature-independent flux noise for commercial SQUIDs at frequencies greater than  $\sim 10$  Hz is

$$S_{\Phi,0}^{1/2} \sim 10^{-6} \Phi_0 / \sqrt{\text{Hz}}, \quad (11)$$

where  $\Phi_0 = h/(2e) = 2.1 \times 10^{-15}$  Wb is the flux quantum. We use this noise level and a fiducial temperature of 0.1 K as our benchmark. DC SQUIDs are also known to exhibit  $1/f$  noise at low frequencies, which can dominate over shot noise below 10 Hz [42]. To be conservative, we limit our discussion to frequencies above 10 Hz, corresponding to  $m_a > 4 \times 10^{-14}$  eV.

Following [25], the signal-to-noise ratio  $S/N$  improves with integration time  $t$  as

$$S/N \sim |\Phi_{\text{SQUID}}| (t\tau)^{1/4} / S_{\Phi,0}^{1/2} \quad (12)$$

for  $t > \tau$ , where  $\tau$  is the axion coherence time.<sup>6</sup> The

<sup>4</sup> We thank Chris Tully for suggesting this strategy to us. For  $N_p$  loops covering the same area as the original loop, the total inductance of the pickup portion of the circuit scales like  $\sim N_p^{-3/2}$ . The mutual inductance  $M_p$  of this arrangement will be small if all the loops are coplanar with the toroid. This is the opposite of a solenoid where the loops are coaxial and connected in series, and similar in spirit to fractional-turn magnetometers [40, 41].

<sup>5</sup> Note that the kinetic inductance of each loop is negligible compared to the geometric inductance.

<sup>6</sup> When  $t < \tau$ ,  $S/N \sim |\Phi_{\text{SQUID}}| \sqrt{t} / S_{\Phi,0}^{1/2}$ .

axion coherence time is approximately

$$\tau \sim \frac{2\pi}{m_a v^2} \sim 10^6 \frac{2\pi}{m_a} \approx 3 \times 10^4 \text{ s} \left( \frac{10^{-12} \text{ eV}}{m_a} \right), \quad (13)$$

where we have taken  $v \sim 10^{-3}$  as the local DM virial velocity. We assume a fiducial integration time of  $t = 1$  year, so that  $t \gg \tau$  over the mass range of interest. Then, requiring  $S/N > 1$  after time  $t$  implies sensitivity to

$$g_{a\gamma\gamma} > 7 \times 10^{-19} \text{ GeV}^{-1} \left( \frac{m_a}{10^{-12} \text{ eV}} \frac{1 \text{ year}}{t} \right)^{1/4} \\ \times \frac{0.88 \text{ m}^3}{V_B} \frac{5 \text{ T}}{B_{\text{max}}} \sqrt{\frac{0.3 \text{ GeV/cm}^3}{\rho_{\text{DM}}}} \quad (14) \\ \times \frac{0.1}{\Phi_{\text{SQUID}}/\Phi_{\text{pickup}}} \frac{S_{\Phi,0}^{1/2}}{10^{-6} \Phi_0/\sqrt{\text{Hz}}}.$$

As shown in Fig. 2, an ideal broadband setup with the benchmark parameters in (14) could probe the QCD axion for  $f_a \lesssim 10^{15}$  GeV, which is not far below the GUT scale. The sensitivity improves for larger magnetic fields or larger toroids; for a toroid with  $R = 4$  m, one can probe the QCD axion at the GUT scale. However, larger experiments are less sensitive to axion masses near  $10^{-6}$  eV because interference effects can partially cancel the axion-sourced flux. Note that the sensitivity increases at *smaller*  $m_a$ , due to the increase in axion coherence time.

*Resonant approach*—We now turn to an analysis of a tuned magnetometer, shown in Fig. 3 (right). This read-out circuit has the advantage of enhancing the signal by the quality factor  $Q$  at the resonant frequency. The tuned circuit is a standard design for detecting small magnetic fields at a given frequency (see e.g. [38]). Similar tuned circuits have been considered before for axion DM detection [22] and dark-photon DM detection [24]; our analysis follows closely those of [24] and [37].

In a practical implementation of an LC circuit with resonant frequency  $\omega = 1/\sqrt{LC}$ , the capacitor has nonzero intrinsic resistance  $R$ . Therefore, the circuit has a finite bandwidth  $\Delta\omega_{\text{LC}} = \omega/Q_0$ , where  $Q_0 = (\omega CR)^{-1}$ . To maximize the axion signal given the expected bandwidth  $\Delta\omega/\omega \simeq 10^{-6}$ , the intrinsic bandwidth of the resonant circuit should be set to  $\Delta\omega_{\text{LC}} = \max[\Delta\omega, 2\pi/\Delta t]$ , where  $\Delta t$  is the interrogation time at this frequency. While  $Q_0 \simeq 10^6$  is optimal for sufficiently large  $\omega$ , smaller  $Q$  values are needed at smaller  $\omega$  to make sure the bandwidth matches the interrogation time. For example, in the strategy of [24] where each  $e$ -fold of frequency is scanned for a time period  $t_{e\text{-fold}}$ , and thus  $\Delta t = t_{e\text{-fold}}/Q_0$ , one must take  $Q_0 = \min[10^6, \sqrt{\omega t_{e\text{-fold}}/2\pi}]$ . Decreasing  $Q_0$ , however, means adding additional resistance to the circuit and thereby increasing the thermal noise.

Alternatively, we can employ the feedback damping circuit of [43, 44], which can widen the intrinsic band-

width of the resonant circuit without introducing additional noise. This allows a large  $Q$  factor at all frequencies while still capturing all of the signal [37]. The intrinsic  $Q_0$  of a niobium superconducting LC circuit is over  $10^6$ , so we assume  $Q_0 = 10^6$  as our benchmark, though larger  $Q_0$  may be possible. The signal flux through the SQUID depends sensitively on the details of the feedback circuit, but our signal-to-noise analysis will not depend on those details, so we treat the feedback circuit as a black box with some inductive coupling  $M$  to the SQUID in Fig. 3 (right).

For  $Q_0$  up to  $\sim 10^8$ , thermal noise in the pickup loop dominates over magnetometer noise (see related studies in [24, 45] and further discussion in the appendix). Once we know that thermal noise is dominant, we can calculate the signal-to-noise ratio without regard to the identity of the black box. Following [24], the axion sensitivity is set by requiring the signal power dissipated in the resonant circuit to be greater than that of the noise. The predicted constraints on  $g_{a\gamma\gamma}$  depend on how much time is spent on each frequency band. We imagine a strategy similar to [24] where each  $e$ -fold of frequency is scanned for a time period  $t_{e\text{-fold}}$ . To compare with the broadband circuit, we take  $t_{e\text{-fold}} = 23$  days to cover 7 decades of mass in the same integration time of 1 year.

At frequency  $m_a$ , the signal and noise powers are

$$P_S = Q_0 \frac{m_a \Phi_{\text{pickup}}^2}{2L_T}, \quad P_N = k_B T \sqrt{\frac{m_a}{2\pi t_{e\text{-fold}}}}, \quad (15)$$

where  $L_T$  is the total inductance of the resonant circuit. Requiring a signal-to-noise ratio of unity implies sensitivity to

$$g_{a\gamma\gamma} > 9 \times 10^{-17} \text{ GeV}^{-1} \left( \frac{10^{-12} \text{ eV}}{m_a} \frac{23 \text{ days}}{t_{e\text{-fold}}} \right)^{1/4} \\ \times \frac{0.88 \text{ m}^3}{V_B} \frac{5 \text{ T}}{B_{\text{max}}} \sqrt{\frac{0.3 \text{ GeV/cm}^3}{\rho_{\text{DM}}}} \frac{10^6}{Q_0} \frac{T}{0.1 \text{ K}} \frac{L_T}{1 \mu\text{H}}, \quad (16)$$

where we have assumed a feedback damping circuit that allows us to keep  $Q_0$  fixed at low masses. At high masses, the feedback damping circuit is not necessary unless  $Q_0 > 10^6$  is achievable.

As illustrated in Fig. 2, the sensitivity increases at *larger*  $m_a$  since the signal power density grows as  $m_a$ .<sup>7</sup> On the other hand, at small masses the broadband approach has a superior projected reach for the same experimental parameters. Thus, the resonant and broadband approaches are complementary.

We introduced a new experimental design that is sensitive to ultralight DM with axion-like couplings to electromagnetism in the mass range  $m_a \in [10^{-13}, 10^{-6}]$  eV.

<sup>7</sup> Parasitic capacitances can enforce a cutoff frequency for the LC circuit [22], though this problem could be mitigated [24].

Most existing axion detection proposals use some kind of resonant enhancement, but we have shown that broadband circuits can have superior sensitivity for lighter axion masses. This conclusion agrees with previous literature establishing that untuned SQUID magnetometers outperform tuned magnetometers at low frequencies [37, 38]; this fact has been exploited in e.g. [46, 47] to detect fT magnetic fields from MRI experiments with biological tissue samples. We expect that a broadband magnetometer could also be relevant for detecting dark photon DM [24], and we look forward to further applications of broadband techniques to light DM detection.

*Acknowledgments*—We thank Asimina Arvanitaki, Dmitry Budker, Marat Freytsis, Peter Graham, David E. Kaplan, Rafael Lang, Mariangela Lisanti, Lyman Page, David Pinner, Surjeet Rajendran, Mike Romalis, and Chris Tully for helpful conversations. YK thanks Adam Anderson and Bill Jones for enlightening discussions regarding SQUIDS. BRS is supported by a Pappalardo Fellowship in Physics at MIT. The work of JT is supported by the U.S. Department of Energy (DOE) under cooperative research agreement DE-SC-00012567, by the DOE Early Career research program DE-SC-0006389, and by a Sloan Research Fellowship from the Alfred P. Sloan Foundation.

### Potential noise sources and experimental details

In our analysis, we estimated the magnetometer noise as (11) and claimed that it dominated in the broadband circuit. This noise level is only a factor of 2 or so above the theoretically predicted temperature-independent floor from current shot noise [38]. The spectral density of shot noise is approximately

$$S_{J,0} = \frac{11}{2} e I_0, \quad I_0 = \frac{\Phi_0}{2L}, \quad (17)$$

where  $I_0$  is the critical current per Josephson junction in an ideal SQUID. This translates into a flux noise of

$$S_{\Phi}^{1/2} = L S_{J,0}^{1/2} = \sqrt{\frac{11}{8}} h L / \sqrt{\text{Hz}}, \quad (18)$$

where  $h$  is Planck's constant. Since the signal and shot noise both scale as  $\sqrt{L}$  (see (9)), the signal-to-noise ratio is largely independent of the SQUID parameters.

In a real implementation of our experimental design, magnetic shielding of the entire apparatus will be necessary to reduce environmental noise. The thermal motion of electrons in the shielding material will itself cause thermal noise, however, with an amplitude proportional to  $1/d$ , where  $d$  is the distance from the shield [48]. With a superconducting shield, this effect is expected to be small because the only source of thermal noise comes from the thin layer of normal material at the outside of the shield.

Moreover, a superconducting shield would significantly reduce static fluxes compared to a normal conductor such as copper. With a sufficiently large shield cooled to sufficiently low temperatures, we expect that shielding noise will be subdominant at frequencies above 1 kHz [49]. As long as the shield dimensions are on the order of the toroid size, the signal flux lines will not be significantly distorted at the center of the toroid, and the signal should be relatively unaffected.

An additional source of noise may arise from the static current creating the toroidal  $B$ -field. In the ideal scenario, this current does not source any magnetic flux through the center of the toroid, which is a benefit compared to the geometry studied in [22]. One reason this is beneficial is that large fields may make it difficult to maintain the pickup loop in a superconducting phase. However, a non-uniform geometry, combined with thermal noise in the toroid, may induce static and time-varying flux through the pickup loop due to a small component of the current which circulates azimuthally. We expect this source of noise to be subdominant in the kHz-GHz range compared to magnetometer noise (in the broadband circuit) or thermal pickup noise (in the resonant circuit). One possibility for addressing the fringe fields is to circulate a biasing current in the toroid to cancel any static flux through the pickup loop, but this may itself introduce additional thermal noise. While we neglect these noise sources in our analysis, it is important to carefully consider them in a real implementation of the detector.

To probe masses below  $4 \times 10^{-14}$  eV, corresponding to frequencies of 10 Hz, one could attempt to modulate the flux signal either by modulating the toroidal  $B$ -field or mechanically modulating the pickup loop. Such modulation would likely lead to additional sources of noise, which must be considered in a practical design.

An interesting similarity between our design and a cryogenic current comparator is that a component of the signal flux is actually generated by a Meissner current on the outer layer of superconducting wire surrounding the toroid. This current is accompanied by an equal and opposite Meissner current on the inner layer which excludes  $B$ -fields inside the wire. We expect that this effect will not significantly reduce our signal, though it may change the details of the magnetic field through the center of the toroid as a function of distance and would need to be simulated in a real experiment.

### Dominance of thermal noise for resonant circuits

When treating the resonant strategy in the body of this letter, we argued that thermal noise in the pickup loop dominates over magnetometer noise. Here, we illustrate this observation using the feedback damping circuit of [43, 44], which is one example of the black box

in Fig. 3 (right) that couples the LC resonant circuit to the SQUID magnetometer. The effect of the feedback circuit is to increase the bandwidth—in our case, to  $\Delta\omega/\omega = \max[10^{-6}, 2\pi/(\Delta t\omega)]$ , where  $\Delta t$  is the interrogation time at frequency  $\omega$ —without increasing the noise. We note that this same conclusion, regarding the dominance of thermal noise, was reached for the case of an inductive shunt circuit with a DC SQUID in [24]. Similarly, [24] considered an AC SQUID readout above 10 MHz, where the SQUID was biased by a microwave-frequency source in order to maintain a sufficiently large  $Q$ , and thermal noise was dominant in that case as well. Experimentally, the dominance of thermal noise has been demonstrated for  $Q$  up to  $10^6$  and  $T$  down to 1.2 K for a mechanical-electrical resonator designed to detect gravitational waves [45].

For the feedback damping circuit, it is useful to generalize Fig. 3 to allow for  $N_s$  turns in the pickup loop, so that the total inductance in the resonant circuit is  $L_T = N_s^2 L_p + L_i$ . Note that the  $N_s$  turns are connected in series as in a solenoid, in contrast to the strategy for reducing inductance in the broadband circuit, where  $N_p$  loops are connected in parallel (see footnote 4). In this circuit, the power spectral density of flux noise through the SQUID,  $S_\Phi(f)$ , at frequency  $f$  contains three contributions [37], namely thermal noise,

$$S_\Phi^T(f) = \frac{4k_B T L_T}{N_s^2 \omega Q_0}, \quad (19)$$

SQUID voltage noise,

$$S_\Phi^V(f) \approx \frac{L_T^2 (\Delta\omega)^2}{N_s^2 \omega^2 M^2 V_\Phi^2} S_V(f), \quad (20)$$

and SQUID current noise,

$$S_\Phi^J(f) \approx \frac{M^2}{N_s^2} S_J(f). \quad (21)$$

Here,  $M = \alpha^2 N_i L$  is the coupling of the input inductor  $L_i$  to the SQUID,  $\omega$  is the resonant frequency,  $\Delta\omega$  is the bandwidth of the resonant circuit including the contribution of feedback damping, and  $Q_0 = (\omega C R)^{-1}$  is the intrinsic quality factor of the capacitor.  $V_\Phi$  characterizes the voltage response of the SQUID to a change in flux, and it is roughly expected to be  $R/L \sim 10^9 - 10^{10} \text{ s}^{-1}$ . For a SQUID of junction resistance  $R$ ,  $S_V(f) \approx 16k_B T R$  and  $S_J(f) \approx 11k_B T/R + S_{J,0}$  are the spectral densities of voltage and current noise [38]. We have explicitly added the irreducible shot noise contribution  $S_{J,0}$  to the SQUID current noise (see (17)); this term is negligible at high temperatures but begins to dominate below  $\sim 60$  mK.

The optimal number of turns in the pickup loop is determined by minimizing the magnetic flux noise through

the SQUID with respect to  $N_s$  [37], yielding

$$N_s^2 L_p = L_i \left[ 1 + \frac{\alpha^2 \omega V_\Phi}{4Q_0 (\Delta\omega)^2} + \frac{\alpha^4 R \omega^2}{16k_B T (\Delta\omega)^2} \left( \frac{11k_B T}{R} + S_{J,0} \right) \right]^{1/2}. \quad (22)$$

For  $\Delta\omega/\omega = 10^{-6}$ ,  $\alpha^2 = 0.5$ , frequencies  $\omega < 10$  MHz, and  $Q_0 > 10^6$ , the last term in (22) dominates, giving  $N_s^2 L_p \approx 10^6 L_i$  and thus  $L_T \approx 10^6 L_i$ .

Depending on the maximum attainable capacitance, the optimal  $N_s$  may be quite large at low frequencies; [37] estimates a maximum low-loss capacitance of 0.1  $\mu\text{F}$ , such that  $N_s \simeq 10^5$  for  $\omega = 10$  Hz, given  $L_p$  as calculated in (10). If the optimal  $N_s$  is too large to be attainable, the single-turn pickup loop inductance  $L_p$  may be changed in order to attain the required  $L_T$  by e.g. decreasing the wire radius  $\phi$  or increasing the radius of the pickup loop  $r$ , both of which may be challenging.

Substituting (22) into (19)–(21) gives

$$S_\Phi(f) \approx \frac{4k_B T L_p}{\omega Q_0} \left[ 1 + \frac{4 \times 10^{-6} Q_0 \Delta\omega}{\alpha^2} \frac{\Delta\omega}{\omega} \frac{1}{V_\Phi} + 10^{-6} Q_0 \alpha^2 \frac{\omega}{V_\Phi} \left( \frac{11}{4} + \frac{S_{J,0}}{4k_B T} \right) \right], \quad (23)$$

where the three terms correspond to thermal noise, SQUID voltage noise, and SQUID current noise. For the parameters of interest, the second term is always subdominant to the third term. Since  $\omega/V_\Phi \lesssim 10^{-2}$ , the third term is suppressed compared to the first for  $Q_0 \lesssim 10^8$ . As discussed in [24],  $Q_0$  for a niobium superconducting LC circuit is at least  $10^6$ , but achieving  $Q_0$  of  $10^8$  is difficult. Thus, thermal noise in the LC resonant circuit dominates the flux noise in the tuned magnetometer below 10 MHz, as anticipated.

It is useful to make contact with the untuned magnetometer in this framework. Ignoring for the moment the finite bandwidth of the signal, as we imagine taking  $Q_0 \rightarrow \infty$  at fixed  $L$  and  $C$ , the resistance in the resonant circuit disappears and magnetometer noise should dominate. Indeed, in that limit the first term in (23) is suppressed, leaving dominantly the current noise, as we found for the broadband circuit:

$$S_\Phi(f)|_{Q_0 \rightarrow \infty} = (11k_B T + S_{J,0}) M^2 / N_s^2. \quad (24)$$

Note that this equation refers to flux noise through the SQUID, and (9) can be used to determine the input flux noise. Also note that  $M^2 \propto N_i^2 \propto N_s^2$ , so that  $S_\Phi$  is independent of  $N_s$  in the broadband case. It is common to take  $N_s = 1$  in order to reduce parasitic resonances [37], and as discussed in footnote 4, there may even be advantages to using a parallel loop setup in the broadband circuit.

\* ykahn@princeton.edu

† bsafdi@mit.edu

‡ jthaler@mit.edu

- [1] John Preskill, Mark B. Wise, and Frank Wilczek, “Cosmology of the Invisible Axion,” *Phys. Lett.* **B120**, 127–132 (1983).
- [2] L. F. Abbott and P. Sikivie, “A Cosmological Bound on the Invisible Axion,” *Phys. Lett.* **B120**, 133–136 (1983).
- [3] Michael Dine and Willy Fischler, “The Not So Harmless Axion,” *Phys. Lett.* **B120**, 137–141 (1983).
- [4] R. D. Peccei and Helen R. Quinn, “CP Conservation in the Presence of Instantons,” *Phys. Rev. Lett.* **38**, 1440–1443 (1977).
- [5] R. D. Peccei and Helen R. Quinn, “Constraints Imposed by CP Conservation in the Presence of Instantons,” *Phys. Rev.* **D16**, 1791–1797 (1977).
- [6] Steven Weinberg, “A New Light Boson?” *Phys.Rev.Lett.* **40**, 223–226 (1978).
- [7] Frank Wilczek, “Problem of Strong P and T Invariance in the Presence of Instantons,” *Phys.Rev.Lett.* **40**, 279–282 (1978).
- [8] Peter Svrcek and Edward Witten, “Axions In String Theory,” *JHEP* **06**, 051 (2006), arXiv:hep-th/0605206 [hep-th].
- [9] Rouven Essig *et al.*, “Working Group Report: New Light Weakly Coupled Particles,” in *Community Summer Study 2013: Snowmass on the Mississippi (CSS2013) Minneapolis, MN, USA, July 29-August 6, 2013* (2013) arXiv:1311.0029 [hep-ph].
- [10] David J. E. Marsh, “Axion Cosmology,” (2015), arXiv:1510.07633 [astro-ph.CO].
- [11] Peter W. Graham, Igor G. Irastorza, Steven K. Lamoreaux, Axel Lindner, and Karl A. van Bibber, “Experimental Searches for the Axion and Axion-Like Particles,” *Ann. Rev. Nucl. Part. Sci.* **65**, 485–514 (2015), arXiv:1602.00039 [hep-ex].
- [12] Stephen J. Asztalos *et al.* (ADMX), “Large scale microwave cavity search for dark matter axions,” *Phys. Rev.* **D64**, 092003 (2001).
- [13] S. J. Asztalos, G. Carosi, C. Hagmann, D. Kinion, K. van Bibber, M. Hotz, L. J. Rosenberg, G. Rybka, J. Hoskins, J. Hwang, P. Sikivie, D. B. Tanner, R. Bradley, and J. Clarke, “SQUID-Based Microwave Cavity Search for Dark-Matter Axions,” *Phys. Rev. Lett.* **104**, 041301 (2010).
- [14] T. M. Shokair *et al.*, “Future Directions in the Microwave Cavity Search for Dark Matter Axions,” *Int. J. Mod. Phys.* **A29**, 1443004 (2014), arXiv:1405.3685 [physics.ins-det].
- [15] J. I. Read, “The Local Dark Matter Density,” *J. Phys.* **G41**, 063101 (2014), arXiv:1404.1938 [astro-ph.GA].
- [16] P. Sikivie, “Experimental Tests of the Invisible Axion,” *11th International Symposium on Lepton and Photon Interactions at High Energies Ithaca, New York, August 4-9, 1983*, *Phys. Rev. Lett.* **51**, 1415–1417 (1983), [Erratum: *Phys. Rev. Lett.* **52**, 695 (1984)].
- [17] Michael Dine, Willy Fischler, and Mark Srednicki, “A Simple Solution to the Strong CP Problem with a Harmless Axion,” *Phys. Lett.* **B104**, 199 (1981).
- [18] A. R. Zhitnitsky, “On Possible Suppression of the Axion Hadron Interactions. (In Russian),” *Sov. J. Nucl. Phys.* **31**, 260 (1980), [*Yad. Fiz.* **31**, 497 (1980)].
- [19] Jihn E. Kim, “Weak Interaction Singlet and Strong CP Invariance,” *Phys. Rev. Lett.* **43**, 103 (1979).
- [20] Mikhail A. Shifman, A. I. Vainshtein, and Valentin I. Zakharov, “Can Confinement Ensure Natural CP Invariance of Strong Interactions?” *Nucl. Phys.* **B166**, 493 (1980).
- [21] K Grohmann, HD Hahlbohm, H Lübbig, and H Ramin, “Current comparators with superconducting shields,” *Cryogenics* **14**, 499–502 (1974).
- [22] P. Sikivie, N. Sullivan, and D. B. Tanner, “Proposal for Axion Dark Matter Detection Using an LC Circuit,” *Phys. Rev. Lett.* **112**, 131301 (2014), arXiv:1310.8545 [hep-ph].
- [23] Scott Thomas and Blas Cabrera, “Detecting string-scale QCD axion dark matter,” Conference talk at Axions 2010.
- [24] Saptarshi Chaudhuri, Peter W. Graham, Kent Irwin, Jeremy Mardon, Surjeet Rajendran, and Yue Zhao, “Radio for hidden-photon dark matter detection,” *Phys. Rev.* **D92**, 075012 (2015), arXiv:1411.7382 [hep-ph].
- [25] Dmitry Budker, Peter W. Graham, Micah Ledbetter, Surjeet Rajendran, and Alex Sushkov, “Proposal for a Cosmic Axion Spin Precession Experiment (CASPER),” *Phys. Rev.* **X4**, 021030 (2014), arXiv:1306.6089 [hep-ph].
- [26] Oliver K. Baker, Michael Betz, Fritz Caspers, Joerg Jaeckel, Axel Lindner, Andreas Ringwald, Yannis Semertzidis, Pierre Sikivie, and Konstantin Zioutas, “Prospects for Searching Axion-like Particle Dark Matter with Dipole, Toroidal and Wiggler Magnets,” *Phys. Rev.* **D85**, 035018 (2012), arXiv:1110.2180 [physics.ins-det].
- [27] Peter W. Graham and Surjeet Rajendran, “Axion Dark Matter Detection with Cold Molecules,” *Phys. Rev.* **D84**, 055013 (2011), arXiv:1101.2691 [hep-ph].
- [28] Peter W. Graham and Surjeet Rajendran, “New Observables for Direct Detection of Axion Dark Matter,” *Phys. Rev.* **D88**, 035023 (2013), arXiv:1306.6088 [hep-ph].
- [29] Dieter Horns, Joerg Jaeckel, Axel Lindner, Andrei Lobanov, Javier Redondo, and Andreas Ringwald, “Searching for WISPy Cold Dark Matter with a Dish Antenna,” *JCAP* **1304**, 016 (2013), arXiv:1212.2970 [hep-ph].
- [30] Dieter Horns, Axel Lindner, Andrei Lobanov, and Andreas Ringwald, “WISPy from the Dark Side: Radio Probes of Axions and Hidden Photons,” in *9th Patras Workshop on Axions, WIMPs & WISPs (PATRAS13) Mainz, Germany, June 24-28, 2013* (2013) arXiv:1309.4170 [physics.ins-det].
- [31] Jooyoo Hong, Jihn E. Kim, Soonkeon Nam, and Yannis Semertzidis, “Calculations of resonance enhancement factor in axion-search tube-experiments,” (2014), arXiv:1403.1576 [hep-ph].
- [32] Christopher T. Hill, “Axion Induced Oscillating Electric Dipole Moments,” *Phys. Rev.* **D91**, 111702 (2015), arXiv:1504.01295 [hep-ph].
- [33] Christopher T. Hill, “Axion Induced Oscillating Electric Dipole Moment of the Electron,” (2015), arXiv:1508.04083 [hep-ph].
- [34] Ariel Arza, Paola Arias, and Jorge Gamboa, “Parametric Resonance and Dark Matter Axion-Like Particles,” (2015), arXiv:1506.02698 [hep-ph].
- [35] Ben T. McAllister, Stephen R. Parker, and Michael E. Tobar, “Axion Dark Matter Coupling to Resonant Photons via Magnetic Field,” (2015), arXiv:1512.05547 [hep-ph].

- ph].
- [36] J. K. Vogel *et al.*, “IAXO - The International Axion Observatory,” (2013) arXiv:1302.3273 [physics.ins-det].
- [37] Whittier Myers, Daniel Slichter, Michael Hatridge, Sarah Busch, Michael Mößle, Robert McDermott, Andreas Trabesinger, and John Clarke, “Calculated signal-to-noise ratio of MRI detected with SQUIDs and faraday detectors in fields from  $10\mu\text{T}$  to 1.5 T,” *Journal of Magnetic Resonance* **186**, 182–192 (2007).
- [38] John Clarke, Claudia D. Tesche, and R.P. Giffard, “Optimization of dc squid voltmeter and magnetometer circuits,” *Journal of Low Temperature Physics* **37**, 405–420 (1979).
- [39] D Shoenberg, *Superconductivity* (Cambridge University Press, 1954).
- [40] JE Zimmerman, “Sensitivity enhancement of superconducting quantum interference devices through the use of fractional-turn loops,” *Journal of Applied Physics* **42**, 4483–4487 (1971).
- [41] D Drung, R Cantor, M Peters, HJ Scheer, and H Koch, “Low-noise high-speed dc superconducting quantum interference device magnetometer with simplified feedback electronics,” *Applied Physics Letters* **57**, 406–408 (1990).
- [42] SM Anton, JS Birenbaum, SR O’Kelley, V Bolkhovsky, DA Braje, G Fitch, M Neeley, GC Hilton, H-M Cho, KD Irwin, *et al.*, “Magnetic flux noise in DC SQUIDs: Temperature and geometry dependence,” *Physical Review Letters* **110**, 147002 (2013).
- [43] HC Seton, DM Bussell, JMS Hutchison, and DJ Lurie, “Use of a DC SQUID receiver preamplifier in a low field MRI system,” *Applied Superconductivity, IEEE Transactions on* **5**, 3218–3221 (1995).
- [44] HC Seton, JMS Hutchison, and DM Bussell, “Gradiometer pick-up coil design for a low field SQUID-MRI system,” *Magnetic Resonance Materials in Physics, Biology and Medicine* **8**, 116–120 (1999).
- [45] Michele Bonaldi, Paolo Falferi, Massimo Cerdonio, Andrea Vinante, Rita Dolesi, and Stefano Vitale, “Thermal noise in a high Q cryogenic resonator,” *Review of scientific instruments* **70**, 1851–1856 (1999).
- [46] Andrei N Matlachov, Petr L Volegov, Michelle A Espy, John S George, and Robert H Kraus, “SQUID detected NMR in microtesla magnetic fields,” *Journal of Magnetic Resonance* **170**, 1–7 (2004).
- [47] Robert McDermott, SeungKyun Lee, Bennie Ten Haken, Andreas H Trabesinger, Alexander Pines, and John Clarke, “Microtesla MRI with a superconducting quantum interference device,” *Proceedings of the National Academy of Sciences of the United States of America* **101**, 7857–7861 (2004).
- [48] S-K Lee and MV Romalis, “Calculation of magnetic field noise from high-permeability magnetic shields and conducting objects with simple geometry,” *Journal of Applied Physics* **103**, 084904 (2008).
- [49] Mike Romalis, private communication.